The Stanford Five-Element Radio Telescope

RONALD N. BRACEWELL, ROGER S. COLVIN, LARRY R. D'ADDARIO,
C. JOHN GREBENKEMPER, KENT M. PRICE, AND ANTHONY RICHARD THOMPSON

Abstract—The Stanford radio telescope array is a fast image-ning interferometer using earth rotation synthesis to produce a brightness map of the continuum radiation from a portion of the sky using data obtained in one 10-h observation. The array consists of five 18.3-m diam paraboloid antennas mounted on an east–west line in such a way that pairs of antennas span all spacings from 1 to 9 times the unit spacing of 22.9 m. At the operating wavelength of 2.8 cm (10 690 MHz) the half-peak beamwidth is 18.8″ and the grating-lobe spacing is 4.2′, both in the east-west direction. The antennas, which were constructed at Stanford, are equatorially mounted and have a range of motion in declination from the south horizon to the north pole and in hour angle from horizon to horizon or ±5 h, whichever is less. Both hour angle and declination motions are controlled by chain-drive mechanisms. The electronic receiving systems includes tunnel-diode preamplifiers followed by mixers and an IF system with a passband from 10 to 70 MHz; both upper and lower sidebands are accepted. The local oscillators at the antennas are phase locked to a reference signal which is distributed from a centrally located oscillator. A system for monitoring variations in the electrical lengths of the reference-signal cables is incorporated using modulated reflectors at the five antennas. The IF signals from the antennas pass through 9-b variable delay lines and the signals from each of the ten possible antenna pairs are then fed into ten analog multipliers. An on-line computer samples the output waveform of each multiplier five times per second and digitally filters the data to estimate the complex correlation of the signals averaged over any desired time interval. The computer also sets the delays, monitors various equipment, and controls the data recording and operator displays. In addition, it can be used off-line to perform the Fourier transformation or similar processing required to derive a map of a radio source. The sensitivity with the tunnel diode preamplifiers gives a signal-to-noise ratio of 5 to 1 for a point source of flux density 4×10^{-28} W $\cdot m^{-2}$ Hz^{-1}; this assumes a system noise temperature of 1000 K, an antenna aperture efficiency of 30 percent, and an observing time of 1 h. An increase in sensitivity by a factor of 10 will be obtained by the use of uncooled degenerate parametric amplifiers.

Introduction

By 1962 the techniques for constructing interferometers with fan beams narrower than a minute of arc had been demonstrated, for example by Swarup, Thompson, and Bracewell [1] and the method of earth-rotation synthesis using fan beams had already been demonstrated by Christiansen and Warburton [2] and analyzed theoretically by Bracewell [3]. In addition, the notion of supersynthesis, a combination of movable antennas and earth rotation had been introduced by Ryle [4], so the time was ripe for the design of new radio telescope systems. Some details of the projects originating about that time are given in Table I.

The high frequency of 10 690 MHz (approximately 2.8 cm) was chosen for the Stanford project, in spite of difficulties that would have to be faced with mechanical precision, because it would be specially suited to studies of the planets, sun, and moon and because, in the case of galactic and extragalactic objects, it would be complementary to the lower frequencies of the instruments being contemplated elsewhere.

The concept of minimum redundancy, which was in the air at the time, was also incorporated, leading to an east–west array of five 18.3-m diam equatorially mounted paraboloids situated at the locations indicated by the numbers as follows, east being on the right.

10 · · 7 · · · 3 2 1.

It will be seen that all interelement spacings from one through nine units are present and that unit spacing occurs twice. The basic design parameters, which were frozen by 1965, were described at the 15th General Assembly of the International Scientific Radio Union in Munich in 1966 [5] and are given in Table II. The general appearance of the array is shown in Fig. 1.

Principle of Operation

The signals from each antenna pair are correlated in the control room by a combination of analog and digital techniques to yield measurements proportional to complex visibility [6] after regular averaging intervals that may be varied but are typically 5 min. On the u–v plane [7], [8], which is the domain related by two-dimensional Fourier transformation to the source domain or "sky plane," nine concentric elliptical loci are traced out as time elapses [9]. If the complex visibility were known everywhere in the u–v plane, Fourier transformation would yield the source distribution;[1] but because data are available only within a central island on the u–v plane, the resolution is limited in a way describable by the shape of the main beam of the instrument. And because within this island only discrete loci are used, there is a further phenomenon of ringlobes surrounding the main beam in the full instrumental response pattern. The character of the main beam and ringlobes of east–west rotation-synthesis arrays has been studied by Bracewell and Thompson [9] with the result for the radial profile of the principal response pattern[2] shown in Fig. 2. The main beam is seen to be accompanied by oscillations which, if we take the squared amplitude, become the fringes that are customary in the intensity diffraction pattern of a circular (or elliptical) aperture. The first two of the series of ringlobes are also shown. Naturally the sidelobes may be reduced to any desired extent by data processing equivalent to the practice of aperture tapering, at the expense of a corresponding reduction in resolving power. The antenna pattern of a single element, which is also shown in this figure, acts to reduce the ringlobe response.

Mechanical System

Each reflector comprises an octagonal steel hub and 56 identical 63-kg aluminum panels, which are made of welded and riveted tube 3.2 cm in diameter and a 1.5-mm reflecting skin. To minimize the amount of material, and hence the cost, the skin was made an integral load-bearing member; this design choice requires accurate and rigid structural work. A heavy optically aligned jig was built to impose the correct double curvature on the skin and fix its spatial relationship to the three points of attachment of the panel to the hub. The skin was formed by bending two 3.66 by 1.22-m sheets with permanent matt-white baked finish, the largest standard size available, over the jig. The sheets were not sheared to pie shapes but used as delivered; what would otherwise have been excess material was formed into flanges for rigidity and to

Manuscript received March 9, 1973. Financial support was provided by the Air Force Office of Scientific Research under Contracts AF49(638)-1375 and F44620-68-C-0028 and by National Science Foundation under Grants GP-4841, GP-7996, GP-8779, GP-9148, and GP-13696 followed by a Grant GP-31382. Preparation and publication of this paper was assisted by the Stanford Joint Services Electronics Program under Contract N00014-67-A-0112-0044.

R. N. Bracewell, L. R. D'Addario, C. J. Grebenkemper, and K. M. Price are with the Radio Astronomy Institute, Stanford University, Stanford, Calif. 94305.

R. S. Colvin is with the Utlie Technology International, Sunnyvale, Calif.

A. R. Thompson is with the National Radio Astronomy Observatory, Charlottesville, Va. 22901.

[1] Corrections may need to be applied for asymmetry of an antenna pair and for the nonzero extent of the antennas since it is the complex degree of coherence of the field, rather than the complex visibility recorded by the apparatus, which is strictly the Fourier transform of the brightness distribution [6].

[2] The principal response pattern is only one of a range of possible patterns that may be synthesized [9].

eliminate gusset plates or connectors at the junctions of the tubes with the skin. Completed panels were cantilevered from their three support points and surveyed by automatic level and self-erecting leveling rods bearing fine scales and resting on conical points. Destruction and deflection tests were carried out by loading with sandbags; the joint design is thus known to be capable of withstanding a wind over 110 km/h blowing normally on the skin. (The rest of the structure was designed for 160 km/h allowing for the known wind loads on solid paraboloids variously oriented. A wind of 110 km/h at a height of 10 m is expected at the site once in 40 years.) The rms surface accuracy of the assembled reflectors after erection is approximately 2 mm, as determined with a theodolite on a built-in mount near the vertex; small target holes were drilled in identical known locations for this purpose while each panel was under construction on the jig.

The feed support is an octopod based on the octagonal steel hub to obtain more rigid support than would be available for the feet of a widely spread tripod or quadrupod. The octopod enables the legs to converge in the focal plane instead of beyond it and together with the low focal ratio (0.3) it leads to a short, light, and rigid feed support. A front-end box and a feed-rotator box are supported at the focus and may be reached for servicing by pointing the antenna to the south horizon. A 4.57-m diam declination wheel is attached to the hub and is driven by a 3-strand chain of 44.45-mm pitch that is held under pretension by compressed elastomers at each end A conventional pinion-driven gear was considered but it was found to be about five times more costly. The declination wheels were assembled identically on a special jig that controlled the interrelationship of the declination bearings and the surface of the circular chainway. The welding was done in conjunction with theodolite observations from concrete mounts. The weight of the reflector and structure that moves with it is 9500 kg.

Attachment of the 56 identical aluminum panels to the welded steel hub had to cope with welding distortion of 5 to 10 mm. Machining of the weldment was considered but as it is approximately 4 m in diam and 2 m high heavy costs would have been incurred. They were circumvented by attaining the circular symmetry which, on smaller pieces, would most naturally be achieved on a lathe. The hub was fabricated on top of a rotating platform; then the panel connectors, which are the only parts demanding circularly symmetrical placement, were welded to the hub while being held rigidly in a jig fixed to the ground. The connecting devices are steel sleeves into which the three tubular panel members were plugged. After welding, the platform was rotated 1/56 of a turn and the operation was repeated. Each panel was then plugged in and adjusted with the aid of the theodolite mount near the vertex of the paraboloid. Tubular members interconnecting the panels were welded into place from a fixed platform with good use again being made of the rotating platform. Frequent theodolite monitoring controlled the sequence of operations and showed that the final adjustments and measurements must be carried out at night because, before the final structural bonds are made, thermal distortion due to sunlight exceeds the 1-mm tolerance desired.

The declination axis is offset by 2.02 m from the hub axis with the result that the lower rim of the reflector is near the ground both when the antenna is in its stowed position (pointing to the north pole) and when it is pointing to the south horizon at its other limit of travel. This feature avoids having to raise the pedestal on 2-m columns, which would more than double the amount of steel in the aready heavy pedestal, and simplifies every operation in which height is a consideration.

A steel yoke supports the reflector on roller bearings, carries the declination drive, and constitutes an hour-angle wheel 9.14 m in diameter around which a 6-strand chain of 38.1-mm pitch wraps. It weighs 17 000 kg including a 9000-kg counterweight, and is in turn supported by a pedestal so as to be able to rotate about a polar axis. The pedestal weighs 4970 kg and is attached to a reinforced concrete foundation consisting of three beams connecting the feet of the pedestal and three columns that descend between 3 and 4 m to firm gravel. Each pedestal has a built-in theodolite mount from which targets may be sighted in corresponding positions on the other pedestals and can also sight targets inside the polar axle and in the ends of the declination axle. An assembly drawing showing a view of a single antenna from the north is given in Fig. 3. Speeds and other details of the two drive systems are summarized in Fig. 4.

Hour angle and declination are indicated in the control room on mechanical counters driven by means of synchros with 18-tooth pinions engaging a fine-pitch (3.33 mm) rack rigidly attached to each chain-driven wheel. The surfaces against which the racks are mounted were built up with epoxy resin and then ground to a predetermined radius after the structures were erected by driving the antenna past grinding wheels fixed to the yoke or pedestal. Counterweights were not included in the original design because the drive motors had to be able to cope with wind loads much larger than the dead weight. For example, the wind load at 80 km/h normal to the reflector is 1.5 times the weight of the reflector. The yoke was, however, partially counterweighted with 9000 kg at a late stage to compenate for low gear-reducer efficiencies that would be encountered should sudden winds require the antennas to be slewed to stow from a cold start. The stow position, with the antennas pointing to the north pole, brings hard points of the steel hub of the reflector into close uxtaposition with the pedestal. The stow locks latch automatically as the antennas drive north on the meridian, forcing the hub down on elastomers on the pedestal.

Expenditure during construction was 2 137 000 dollars made up of sarlaries 793 000 dollars, overhead and staff benefits 515 000 dollars, equipment, materials, services, and supplies 538 000 dollars, computing 45 000 dollars, other 245 000 dollars. Other programs were conducted at the same time; the cost of the array itself is estimated at 1 900 000 dollars.

All the mechanical and structural work was done on the site by the personnel of the Stanford Radio Astronomy Institute [10]. Photographs, drawings, and other details of the construction have been presented elsewehre [11] Mechanical drawings and over 100 technical reports may be consulted at Stanford, and an index to the reports is available on request.

The Receiving System

A block diagram of the electronic receiving and data processing system is shown in Fig. 5. To follow the diagram note that the horizontal dashed lines separate the front-end

box which is mounted near the focus, the ground box at the base of the antenna, the delay room, and the control room. The components in the front end and ground boxes are shown for one antenna only.

Front End

The signal is received at a linearly polarized feed horn, remotely rotatable to any desired angle of polarization, at the focus of each paraboloid. Modulated noise is added to the signal to permit measurement of the overall gain and then, in the normal mode of operation, it is directly connected to a tunnel-diode amplifier. An alternative mode can be selected by the waveguide switch so that the signal and a matched load at ambient temperatures are connected alternately to the amplifier at 35 Hz by a Dicke switch. This makes possible total-power measurements with a single antenna for calibration of pointing, aperture efficiency, etc. The amplifiers, which were obtained in the years 1967–1968, have a noise temperature of 900 K and were intended to provide a test system to be replaced by degenerate parametric amplifiers with noise temperatures around 90 K. Both sidebands of the amplifier signal are converted by a mixer to a band which extends from 10 to 70 MHz, and after further amplification the IF band is transmitted underground to the thermally stable delay room through a pressurized semi-air-spaced cable (1.27-cm Sprioline). The double-sideband system is appropriate for the future addition of degenerate parametric amplifiers and has the advantage that phase changes in the IF cables do not affect the phase of the multiplier output waveforms.

Synchronized Local Oscillator

The 10.690-GHz local oscillator at each antenna is a Gunn-diode unit phase locked to the 10.693-GHz fourth harmonic of a signal at 2673.25 MHz coming from a 0.5-W crystal-controlled oscillator in the control room. A 3.0-MHz reference signal is also distributed to each antenna for comparison with the difference frequency between the local oscillator and the fourth harmonic. The 2673.25-MHz transmission line is a pressurized 2.22-cm diam semi-air-spaced cable which is buried between the control room and the base of each antenna, and, on the exposed run from the ground to the focus, is covered by a sponge-rubber thermally insulating tube encased in an aluminum outer pipe.

Phase Monitoring

Thermal changes in the electrical lengths of the cables can be monitored using the system on the right-hand side of Fig. 5. A small modulated component of the 2673.25-MHz reference signal is reflected back down the line by a diode switch located in the front-end box and driven by a 400-Hz square wave. The reflected signal comes out of the lower port of the circulator where it is then mixed in a dectector with a sample of the outgoing signal, the phase of which can be varied by a calibrated phase shifter. The switch-frequency waveform from the detector output is amplified, synchronously detected, and displayed on a meter. When the phase shifter is set for zero output on the meter, the phase of the reference sample is in quadrature with the reflected component, and the setting of the phase shifter thus gives a measure of any variation in the round-trip path out to the reflector and back. A small component of the outgoing signal can also reach the detector through the reverse path in the circulator and could cause an error in the indicated phase. This component is canceled by adjustment of the tuner; before a phase measurement is made, the modulating square wave is switched to the diode switch at the lower port of the circulator, the connection between the phase shifter and the hybrid is opened, and the tuner is set for minimum reading of the phase detector output. Use of the phase-monitoring system does not disturb observations in progress and provides an accuracy equivalent to 3° of phase at the local-oscillator frequency. It has been found that line lengths vary only slowly in time, the total change in 10 h rarely exceeding 15°. The method was introduced by Swarup and Yang [12] for the Stanford microwave spectroheliograph.

Wide-Band Variable Delays

Because of the wide bandwidth, compensation has to be made for the fact that the antennas are at different distances from the source under study; otherwise there would be a loss in sensitivity from reduced correlation of the signals received from different antennas. Variable delay units equalize the time delays in the five signal paths from the source to the multipliers to within about 1 ns, which is 1/20 of the reciporcal IF bandwidth. A fixed delay is used for the antenna at position number seven, the nearest one to the center of the array, and an on-line computer controls the other four delays as a source is tracked across the sky. Each delay unit has 512 different possible delays obtained by switching in lengths of 1.27-cm semi-air-space dcable. Each length, when switched out, is replaced by a short piece of high-loss cable of equal attenuation. The cable lengths in each unit are proportional to the spacing of the corresponding antenna from number seven. All units are switched simultaneously by a reed-relay system designed by Little.

IF Amplifiers

The IF amplifiers in the control room provide 45 dB of gain to compesnate for losses in the delay units and IF transmission cables and their frequency response is adjusted to compensate partially for the difference in cable attenuation across the passband. Automatic level-control loops in the IF amplifiers hold their output levels constant, compensating for small attenuation changes which may occur when delay cables are switched. The overall gain of any of the five receiving channels may be measured at any time by switching a small portion of the IF amplifier output into a gain-monitoring receiver which measures the strength of the modulated noise injected at each front end; this is accomplished by a synchronous detector driven in phase with the modulation. Finally, each IF amplifier output is divided four ways, providing 20 inputs controlled at 20 mV rms for the ten analog multipliers.

Wide-Range Multipliers

In each of the multiplier units the multiplying element consists of two transistors with a common emitter resistor; the basic circuit, which has been described by Frater [13], was proposed for our use by Aitchison. In this application transistors were found to provide a higher dynamic range than diodes, an important consideration for observation of a strong source, such as the sun, for which a large fraction of the noise at the multiplier inputs is correlated. Within each multiplier unit one input signal is phase switched and the voltage from the multiplying transistors is amplified at the switching frequency and synchronously detected. The multiplier outputs are sampled by an analog multiplexer which is switched from one output to the next at a rate of 50 Hz. A resistance–capactiance filter at the output of each multiplier limits the noise bandwidth to about 2 Hz and samples are

then taken at 5 Hz. The signals at this point are quasi-sinusoidal "fringes" with a minimum period of 1.87438 s, which is reached where the declination δ and hour angle h are both zero and then n is 9 units. In general, the nominal fringe period is 1.87438 $(9/n)$ sec δ sec h. A voltage-to-frequency converter and counter provide analog-to-digital conversion of the sampled voltages, which are then fed into the computer. The output of any one of the multipliers can also be displayed on a chart recorder for monitoring purposes.

The On-Line Computer

The computer is a Hewlett Packard Model 2114B, which is a 16-b machine with 8192 words of memory and a 2.0-μs cycle time. It performs four main tasks in on-line operation: control of the data sampling and reduction of the multiplier outputs to estimates of complex visibility; recording and display of the visibility data and system parameters; computation and display in real time of the desired antenna positions, taking into account calibrated pointing errors; and control of the delay lines. The first of these is the most complex, and will be discussed in more detail in what follows. The operator interacts with the system through a cathode-ray tube (CRT) terminal, from which he can enter data and can command without interrupting any ongoing data sampling. Other inputs to the computer include a digital sidereal clock and a multichannel scanner, the latter being used to monitor various equipment parameters. Mass storage is provided by a cassette-type magnetic tape unit with three transports. Final data reduction can be performed off line on the same computer or at the Stanford Computation Center to which data can be transmitted via telephone lines.

It can be shown that the output signal $s(t)$ from each multiplier, after low-pass filtering to a bandwidth much less than the IF bandwidth, may be expressed as

$$s(t) = V_R \cos(2\pi D/\lambda) + V_I \sin(2\pi D/\lambda) + n(t) \quad (1)$$

where V_R and V_I are the real and imaginary parts, respectively, of the quantity, proportional to complex visibility, measured by the corresponding antenna pair; $n(t)$ is a zero-mean Gaussian noise process; and D is the path difference for a reference direction r given by

$$D = r \cdot L + p_1(r) - p_2(r). \quad (2)$$

Here r is a unit vector, L is the spacing between two corresponding earth-fixed reference points at the two antennas, and $2\pi p_1/\lambda$ and $2\pi p_2/\lambda$ are the phase differences between the fields at each reference point due to waves coming from the direction r and the signals at the terminals of the corresponding antenna. If the reference points are chosen carefully, p_1 and p_2 will vary only slowly with r (further discussion of this is given in a later section). Rotation of the earth causes r (and consequently D) to vary with time in such a way that $s(t)$ may be described as quasisinusoidal with slowly changing frequency. Samples of $s(t)$ for each multiplier are digitized and read into the computer every $\Delta = 0.2$ s. The computer estimates V_R and V_I from a finite sequence of $M+1$ samples, $s(t_0), \cdots, s(t_M)$, $t_i = t_0 + i\Delta$. It is easy to show that if $D(t_M)/\lambda - D(t_0)/\lambda$ is an integer (the samples span an integral number of "cycles" of $s(t)$), then the minimum mean-square error (mmse) estimates are

$$\hat{V}_R = \frac{1}{M+1} \sum_{i=0}^{M} s(t_i) \cos[2\pi D(t_i)/\lambda]$$

$$\hat{V}_I = \frac{1}{M+1} \sum_{i=0}^{M} s(t_i) \sin[2\pi D(t_i)/\lambda]. \quad (3)$$

If a nonintegral number of cycles is spanned, the mmse estimates are more complicated, and they have a somewhat larger variance per sample [14]. The variance increases rapidly if less than one cycle is spanned so the present on-line program ensures that the condition

$$D(t_M)/\lambda - D(t_0)/\lambda = \text{integer}$$

is satisfied; but otherwise M may be freely selected by the observer. The choice of M, or equivalently the "integrating period" $M\Delta$, is also governed by sampling considerations in the u–v plane; for a source whose diameter equals the ringlobe radius of 4.2′, the most widely spaced antenna pair samples an independent point in the Uv-plane every 25 min.

The program evaluates the sine and cosine of $2\pi D(t_i)/\lambda$ in real time, accumulating the sums in (3) separately for each multiplier. Stored information on L for each antenna pair and $p(r)$ for each antenna is used; the reference direction r is computed from the right ascension and declination of date for the center of the source (as entered by the operator) and from the current reading of the sidereal clock.[3] In addition, the quantities

$$\sum_{i=0}^{M} s(t_i) \quad \text{and} \quad \sum_{i=0}^{M} s^2(t_i)$$

are accumulated as a basis for monitoring the dc drift of the multipliers and the system noise, respectively. With ten multipliers, the processing of each sample must be completed in at most $\Delta/10 = 20$ ms. Careful programming was required to achieve this, since hardware multiply and divide instructions were not available. At present, about 65 percent of the available time is used. The computer's priority interrupt system is used to control the sampling, so that all of this processing normally takes place in the "background," while in the "foreground" other tasks are performed, using the remaining 35 percent of the machine's time. These tasks include recording and displaying the data from the preceding integrating period; computing the current desired antenna position settings and displaying them to the operator; monitoring the states of various equipment, and issuing warning messages in case of difficulty; accepting commands and data from the operator; and calibration of the previous integration, using data from an earlier observation of a calibration source, and recording and displaying the results. It is expected that additional capabilities will be added, including plotting of the one-dimensional brightness distribution estimated from calibrated data taken in the last integrating period.

The estimation of the two-dimensional brightness distribution from a 10-h observation must be performed off line because of the computer's limited memory. Programs are available for the 2114B to apply more precise corrections to the visibility data than is possible in the on-line program, taking

[3] Local sidereal time at one end of the array differs from that at the other end by 0.56 s, which can be a nonnegligible fraction of a fringe period (minimum value 1.87 s), but this has no effect on the estimated phase provided r and all the L are referred to the same coordinate frame

into account the effects of atmospheric refraction, small errors in the sidereal clock's setting, etc.; to calibrate the visibility data using any available calibration source observations; to average the data in various ways; to plot estimates of the one-dimensional integrated brightness distribution; and to compute the two-dimensional brightness distribution by taking the direct Fourier transform. If a 5-min integrating time is used, about 1 h is required to complete all of the processing needed to compute the two-dimensional map.

Calibration and Observation Procedures

Pointing Errors

Changing gravitational loads, as an antenna drives across the sky from boundary to boundary, results in movement of the beam through calibratable angles which, at extremes, may be 30′ greater than the drive wheel rotations which the readout system displays.

An observing technique which allows rapid precise measurement of the pointing errors has been developed. It involves tracking an unresolved source with the entire array pointed sequentially at four positions surrounding an initial guess at the correct pointing. All ten magnitudes $(\hat{V}_R^2+\hat{V}_I^2)^{1/2}$ are then recorded, and from the resulting 40 numbers it is possible to determine (with some redundancy) the five two-dimensional pointing errors. This is done by noting that

$$A_{ij} = \text{const} \times [g(\theta_i)g(\theta_j)]^{1/2}$$

where A_{ij} is the visibility magnitude for the channel involving antennas i and j; θ_i, θ_j are the magnitudes of corresponding pointing errors; and $g(\cdot)$ is the power pattern of an individual antenna (assumed known). After writing this set of equations for each of the four observing positions and taking ratios to eliminate the unknown constants, one obtains a nonlinear system which can easily be solved for each $g(\theta_i)$ and then for each θ_i provied $g(\cdot)$ is known.

It is believed that most of the pointing error occurs in the mount structure rather than in the paraboloid or feed support With the result that, considering the lack of simple symmetries with respect to the local vertical, the pointing error for each antenna is a complicated function of direction in the sky. In order to allow real-time prediction of the desired pointing, the following formulas for Δh (indicated minus true hour angle) and $\Delta\delta$ (indicated minus true declination), which are based on structural analysis, were fitted to observational data obtained at numerous declinations.

$$\Delta h = a_1 + a_2 h + a_3 \sin h + a_4 \cos h + a_5 \sin h \sec \chi + a_6 \sin h \tan \delta + a_7 \cos h \tan \delta + a_8 \tan \delta$$

$$\Delta\delta = a_9 + a_{10}\delta + a_{11} \sin h + a_{12} \cos h + a_{16}Q + a_{13}Q \sec \chi$$

where δ is the declination, h is the hour angle, χ is the zenith distance, b is the latitude, $Q = \sin b \sec \delta - \cos \chi \tan \delta$, and the a_i are coefficients determined by a least mean-squares fit.

The coefficients are determined separately for each antenna, and are kept in the core memory of the computer during observations. These expressions maintain the residual pointing errors well within a small fraction of the 7′ beamwidth as shown in Fig. 6. Analysis of such data for a wide range of declinations reveals that systematic errors have been held to 1′ in the worst part of the sky and that random errors have an rms value of 0.5′ (or less, as much of the scatter such as that seen in Fig. 6 could be reduced by repeated observation). Although we regard these as negligible errors for most purposes, they will be reducible even further by refinement of the preceding formulas as we accumulate additional data, a virtue shared with all interferometers having fixed elements. A small pointing error θ reduces the single-element gain by about $\exp(-a\theta^2)$, which for $\theta = 1'$ equals 0.94 (in our case where $a = 0.057$). A random error with standard deviation σ can be shown to reduce the mean signal by a factor $(1+2\sigma^2 a)^{-1/2}$, which equals 0.99 for $\sigma = 0.5'$. This pointing accuracy shoud allow operation with the even narrower single-element beamwidth such as would result at a shorter wavelength of, say, 1 cm.

Focusing

The feed horn of each antenna is fixed at an optimum focus position that was determined by observing the response to a calibration source and using a remotely controlled focuser which was mounted on each antenna in turn.

Phase Calibration

The phase of the estimated complex quantity $\hat{V}_R + j\hat{V}_I$ depends, in accordance with (3), on knowledge of the path difference D. To know D it is necessary to know the relative positions of the reference points fixed with respect to the antenna pedestals, dimensional discrepancies between the two antenna structures such as differences in the distance between the declination and polar axes, and misalignments such as the polar axis not being parallel to the earth's axis. Great care was taken in the construction to make the five antennas as identical as possible and to harmonize the design with surveying requirements. Consequently, all the imperfections are small. Their effects have been analyzed for equatorial mounts such as ours by Wade [15], and the combined effect may be determined by radio source observations and may be expressed in terms of a set of phase parameters from which the path difference D, or phase function D/λ, may be evaluated in real time. As the antennas are permanent objects in permanent locations the parameters may be progressively refined by means of observations of known sources so that the on-line path difference is now accurate to 0.05 wavelengths over the whole sky. Even more precise corrections are possible with off-line computations for special cases.

Because the paraboloid axis does not intersect the declination axis, a path difference is introduced of 0.02 wavelengths per minute of arc differential setting error in declination. The antennas can easily be set to this accuracy. The phase shift in the distribution system of the local-oscillator reference signal is easily held constant to 0.01 cycles using the modulated-reflector phase-monitoring system previously described, thereby reducing the frequency with which calibration sources need be observed.

Observing Procedure

During the course of an observing session, one or more short measurements are made on calibration sources (unresolved sources at known positions, preferably with known flux densities) and these measurements are automatically ap-

indicate brightness temperatures in the range 10^6 to 10^7 K at 2.8 cm and angular widths from 8″ to 25″ in agreement with the dimensions of associated sunspot umbras. A program of observations of Jupiter has begun with a view to studying the radiation belt and its time changes.

In addition to its performance in mapping, the array has a very useful capacity for observations of faint unresolved sources such as quasars, stars, and X-ray sources. It has also been used by D'Addario and Stull [19] to follow the decrease in the flux density of Cygnus X-3 from a value of 1.86×10^{-26} W·m^{-2} Hz^{-1} when first observed after its outburst in September 1972, down to below a level of 0.2×10^{-26} W·m^{-2} Hz^{-1}. The array is clearly well suited to monitoring variations in sources with flux densities of $\sim10^{-26}$ W·m^{-2} Hz^{-1}, and since the addition of parametric amplifiers would increase the sensitivity by an order of magnitude, it is potentially a very useful instrument for variable-source studies. Addition of other wavelengths in the range 1 to 10 cm will allow analysis of Faraday rotation in different parts of extended sources and may lead to critical tests of models for extragalactic and galactic variable sources.

Appendix

Less than Twelve-Hour Tracking

The hour angle notion of the existing structure is limited to $\pm$ h, and in addition, for southern declinations, the motion is further limited by the horizon, so we are led to consider the effect of missing sectors on the u–v plane. The effect is expressible in terms of a correction pattern $p_c(x, y)$ to be subtracted from the pattern shown in Fig. 2. It is easy to compute numerically for any given circumstances but an approximate analytic expression can also be given. Let the missing sectors on the u–v plane have a semivertical angle θ. Then replacing each missing arc by a straight line segment through the centroid of the arc, and retransforming, we obtain

$$p_c(x, y) = (90\pi)^{-1} \sum_{n=1}^{9} 4n\theta \,\mathrm{sinc}\,(2n\theta x) \cos(2\pi\eta n y)$$

where $\eta = (\sin\theta)/\theta$. For 10-h tracking ($\theta = \pi/12$) this expression accurately indicates the correction pattern. Its central value is then 1/6 of that of the 12-h pattern.

Acknowledgment

The project benefited in its construction phase from the interest and advice of Dr. M. Harrington and Dr. L. Wood of AFOSR and of Dr. E. Hurlburt of NSF. Their cooperation made it possible to complete this complex modern instrument at a total cost to the sponsors including all salaries and overhead of 1.9 million dollars. The authors grateful to W. E. Scott who produced the shop drawings of the yoke, pedestal, and machinery packages, C. C. Lee who supervised the mechanical construction until mid-1969, and to A. G. Little who made a major contribution to the design and construction of the readout and delay systems while on sabbatical leave from Sydney University. Further details of personnel are to be found in the Reports of Observatories [10].

[4] The term signal-to-noise ratio is commonly applied to the quasi-sinusoidal output of a multiplying interferometer to mean $S/\Delta S$, where "fringe amplitude" S is expressible in terms of the computable quantities $\hat{V}_R$ and $\hat{V}_I$ by $S = (\hat{V}_R^2 + \hat{V}_I^2)^{1/2} = |\hat{V}|$ and ΔS is the rms multiplier output averaged for time τ in the absence of signal. It can be shown that, when $S/\Delta S \gg 1$, $\Delta v/|\hat{V}| = \sqrt{2}\,\Delta S \gg S$.

plied by the computer to determine the absolute phase and gain of each of the ten interferometer channels. Subsequent variations can be monitored using the modulated reflector and modulated noise source systems shown in Fig. 5. The on-line program can, at the option of the operator, apply corrections for the measured variations, apply the calibrator data, and display the results. Thus we have fully calibrated data available immediately at the end of an observing session. In addition, we record the uncorrected data in case the observer wishes to apply other corrections in the off-line processing.

Sensitivity

Consider the output sinusoid from any one multiplier when the array is observing a point source of flux density F. After an integrating time τ the estimated quantity $\hat{V} = \hat{V}_R + j\hat{V}_I$ has a standard deviation $\Delta V = \langle|\hat{V} - \langle\hat{V}\rangle|^2\rangle^{1/2}$, due to receiver noise given by

$$\frac{\Delta V}{|\hat{V}|} = \frac{2kT_{sys}}{AF(B\tau)^{1/2}}.$$

Here k is Boltzmann's constant, B is the effective bandwidth, and T_{sys} and A are the system noise temperature and the antenna collecting area, which are assumed to be the same for each antenna. Discussions of the signal and noise levels in a multiplying radiometer from which the above formula may be derived are given by Tiuri (see [16], [17]). If N antenna pairs are available simultaneously, the sensitivity is increased by a factor $\sqrt{N}$ since for a point source in the reference direction the visibility is the same for all antenna pairs whereas the errors are independent. If we follow the convention that the minimum observable flux density F_{min} corresponds to a signal-to-noise ratio[4] of 5

$$F_{min} = \frac{5\sqrt{2}\,T_{sys}}{A(NB\tau)^{1/2}}.$$

For the present array $T_{sys} = 10^3$ K, $B = 60$ MHz, $\tau = 10$ h, $N = 10$, and $A = 79$ m^2 (aperture efficiency = 30 percent) and we obtain $F_{min} = 0.03\times10^{-22}$ W·m^{-2} Hz^{-1}. For an extended source an approximate indication of the minimum strength for useful mapping is obtained by requiring a flux density F_{min} from each area of the source that subtends a solid angle equal to that of the synthesized beam.

Fields of Application

From the above figures we estimate that there are about 50 extragalactic sources with measurable structures which can be investigated with the original tunnel-diode amplifiers. Many of these have been mapped at longer wavelengths and interesting studies of the variation of the spectral index should be possible.

The short operating wavelength of the array is also particularly well suited to observations of thermal sources and a program to search for compact components in over 200 H II regions was completed in the summer of 1972 by Felli, Tofani, and D'Addario [20]. The observations were made near meridian transit, providing one-dimensional strip-integrated profiles in only 5 to 10 min of observing time per source. Mapping of galactic and extragalactic sources is continuing, as are observations of the structure of active solar regions. Preliminary solar studies by Grebenkemper and Rust [18]

References

[1] G. Swarup, A. R. Thompson, and R. N. Bracewell, "The structure of Cygnus A,", *Astrophys. J.*, vol. 138, pp. 305–309, July 1963.

[2] W. N. Christiansen and J. A. Warburton, "The distribution of radio brightness over the solar disk at a wavelength of 21 centimeters. III. The quiet sun—two-dimensional observations," *Aust. J. Phys.*, vol. 8, pp. 474–486, Dec. 1955.

[3] R. N. Bracewell, "Strip integration in radio astronomy," *Aust. J. Phys.*, vol. 9, pp. 198–217, June 1956.

[4] M. Ryle, "The new Cambridge radio telescope," *Nature*, vol. 194, pp. 517–518, May 1962.

[5] *Progress in Scientific Radio* (National Academy of Science-National Research Council Publication 1468), pp. 242–244, 1966.

[6] R. N. Bracewell, "Radio interferometery of discrete sources," *Proc. IRE*, vol. 46, pp. 97–105, Jan. 1958.

[7] R. N. Bracewell, "Two-dimensional aerial smoothing in radio astronomy," *Aust. J. Phys.*, vol. 9, pp. 297–314, Sept. 1956.

[8] E. B. Fomalont, "Basic principles and practice at NRAO," this issue, pp. 000–0000.

[9] R. N. Bracewell and A. R. Thompson, "The main beam and ring-lobes of an east-west rotation-synthesis array," to be published in *Astrophys.* J., vol. 182, pt. I, May 1973.

[10] R. N. Bracewell, "Stanford Radio Astronomy Institute," *Astronom. J.*, vol. 72, p. 1274, Dec. 1967; *Bull. Amer. Astronom. Soc.*, vol. 2, no. 1, pp. 134–135, 1970; vol. 3, no. 1, pt. II, p. 192, 1971.

[11] R. N. Bracewell, R. S. Colvin, K. M. Price, and A. R. Thompson, "Stanford's high-resolution radio interferometer," *Sky and Telescope*, vol. 42, pp. 4–9, July 1971.

[12] G. Swarup and K. S. Yang, "Phase adjustment of large antennas," *IRE Trans. Antennas Propagat.*, vol. AP-9, pp. 75–81, Jan. 1961.

[13] R. E. Frater, "Accurate widdband multiplier square-law detector," *Rev. Sci. Instrum.*, vol. 35, pp. 810–813, July 1964.

[14] R. S. Colvin and L. R. D'Addario, "The Stanford five-element array," at NRAO Symp. on Astrophysical Data, Nov. 1972, to be published in *Astron. Astrophys.*,

[15] C. M. Wade, "Precise positions of radio sources. I. Radio measurements," *Astrophys. J.*, vol. 162, pp. 381–390, Nov. 1970.

[16] J. D. Kraus, *Radio Astronomy*. New York: McGraw-Hill, 1966, p. 255.

[17] W. N. Christiansen and J. A. Högbom, *Radiotelescopes*. London, England: Cambridge Univ. Press, 1969.

[18] C. J. Grebenkemper and D. M. Rust, "Solar high-resolution radio measurements of active regions at a wavelength of 2.8 cm." *Bull. Amer. Astronom. Soc.*, vol. 5, p. 21, Jan. 1973.

[19] L. R. D'Addario and M. A. Stull, "Observations of Cygnus X-3 at 2.8 cm with a 17″ beam," *Nature (Phys. Sci.)*, vol. 239, pp. 120–121, Oct. 23, 1972.

[20] M. Felli, G. Tofani, L. R. D'Addario, in preparation.

[21] D. E. Hogg, G. H. McDonald, R. G. Conway, and C. M. Wade, "Synthesis of brightness distribution in radio sources," *Astronom. J.*, vol. 74, pp. 1206–1213, Dec. 1969.

[22] W. N. Christiansen and K. J. Wellington, "A new radiotelescope of 40 sec.-of-arc resolving power for southern sky observations," *Nature*, vol. 209, pp. 1173–1176, Mar. 19, 1966.

[23] W. N. Christiansen, "A new southern hemisphere synthesis radio-telescope," this issue, pp. 0000–0000.

[24] J. W. M. Baars, *et al.*, "The synthesis radio telescope at Westerbork," this issue, pp. 0000–0000.

[25] B. Elsmore, S. Kenderdine, and M. Ryle, "The operation of the Cambridge one-mile diameter radio telescope," *Mon. Not. Roy. Astronom. Soc.* vol. 134, pp. 87–95, 1966.

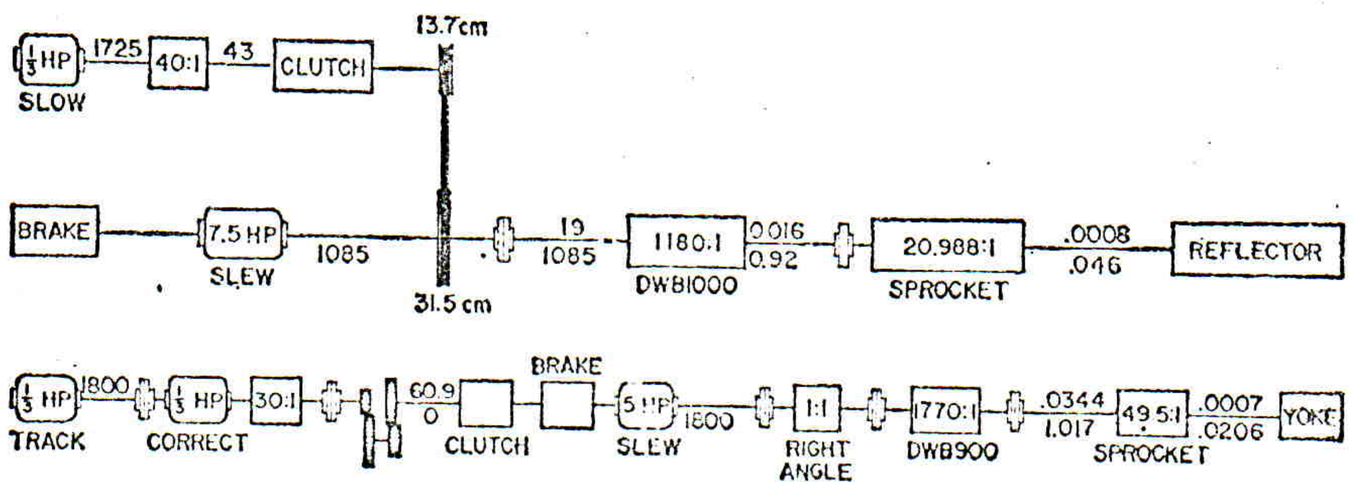

Fig. 4. Drive systems for declination (above) and hour angle (below). Gear ratios are shown in the boxes and shaft speeds in revolutions per minute are shown on the shafts.

TABLE I

CENTIMETER-WAVELENGTH EARTH ROTATION SYNTHESIS ARRAYS

Location	f (MHz)	Elements (total movable)		Diameter (m)	Element Spacing (m)	Maximal Spacing (m)	Beam width	Imaging Time[a] (h)	lobe Radius	Beam of Element
Stanford, Calif.	10690	5	0	18	23	206	19″	10	4′.2	7′
Cambridge, England	5000	8	4	13	40	4560	2″	192[a]	5′	6′
Green Bank	2695	3	2	26	100 and 300	2700	8″	108[a]	4[a]	20′
W. Va. [21]	8085						3″		1′	7′
Big Pine, Calif.	1420	3	3	27 and 40	30.5	1080	7″		24′	33′
Fleurs, Australia [22, 23]	1415	68	0	5.7 and 13.6	12.2	800	40″	12	1°	3°
Westerbork, The Netherlands [24]	610	12	2	25	144	1600	56″	12	23′	83′
	1415						24″		10′	36′
	4995						68″		28′	11′
Cambridge, England [4], [25]	408	3	1	18	12	1550	80″	768[a]	None	3°
	1407						23″			1°

[a] Excluding time taken to move antennas

TABLE II

BASIC PARAMETERS

Latitude[a]	+37°23′55.0″
Longitude[a]	+8h 08m 45.44s
Elevation	70 m
Wavelength in vacuo	2.80441 cm
Frequency	10,690 MHz
IF band	10–70 MHz
Reflector diameter	18.3 m
Element spacing	22.860 m (= 815.146 λ)
Extreme spacing	205.740 m (= 7336 λ)
East–west width of fan beam to half peak[b]	16.1″
East–west width of synthesized beam[b]	18.8″
Beamwidth of single reflector	7′
East–west ringlobe radius[b]	4.2′
Declination axis to polar axis	2.5908 m
Declination axis to paraboloid axis	2.02 m
Declination wheel readout radius	2.0864 m
Hour wheel readout radius	4.633 m

[a] The position given is the intersection of the meridian through the USCGS bench mark RATEL and the parallel, 13.1 m north of the bench mark, passing through the theodolite seats built into the pedestals. The midpoint of the array is 17.2 m west. The observatory location quoted in the American Ephemeris is the center of the adjacent microwave spectroheliograph cross array.

[b] North–south values are larger by the cosecant of the declination.

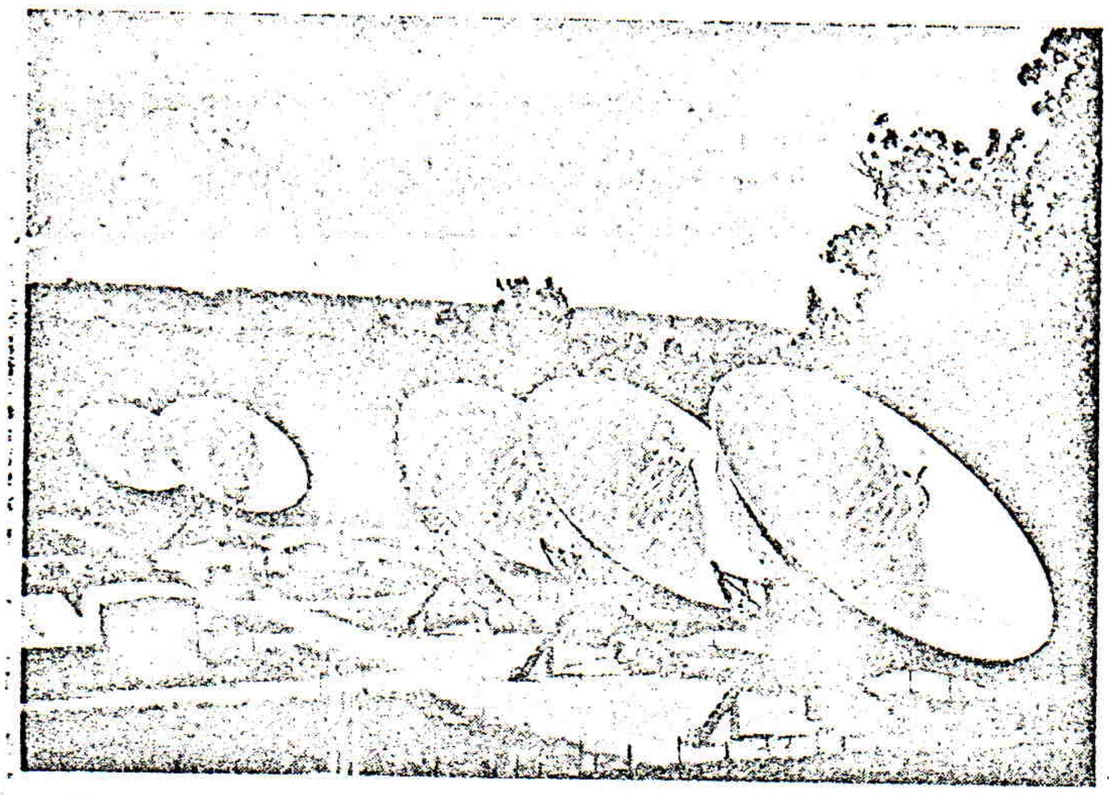

Fig. 1. A photograph of the radio telescope from the south-east.

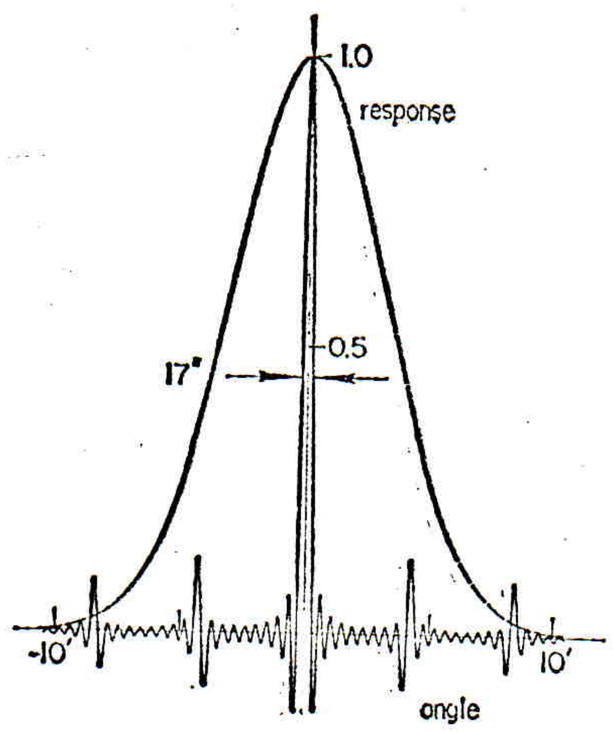

Fig. 2. Radial profile of the principal response pattern (full curve) and of the pattern of a single element (broken).

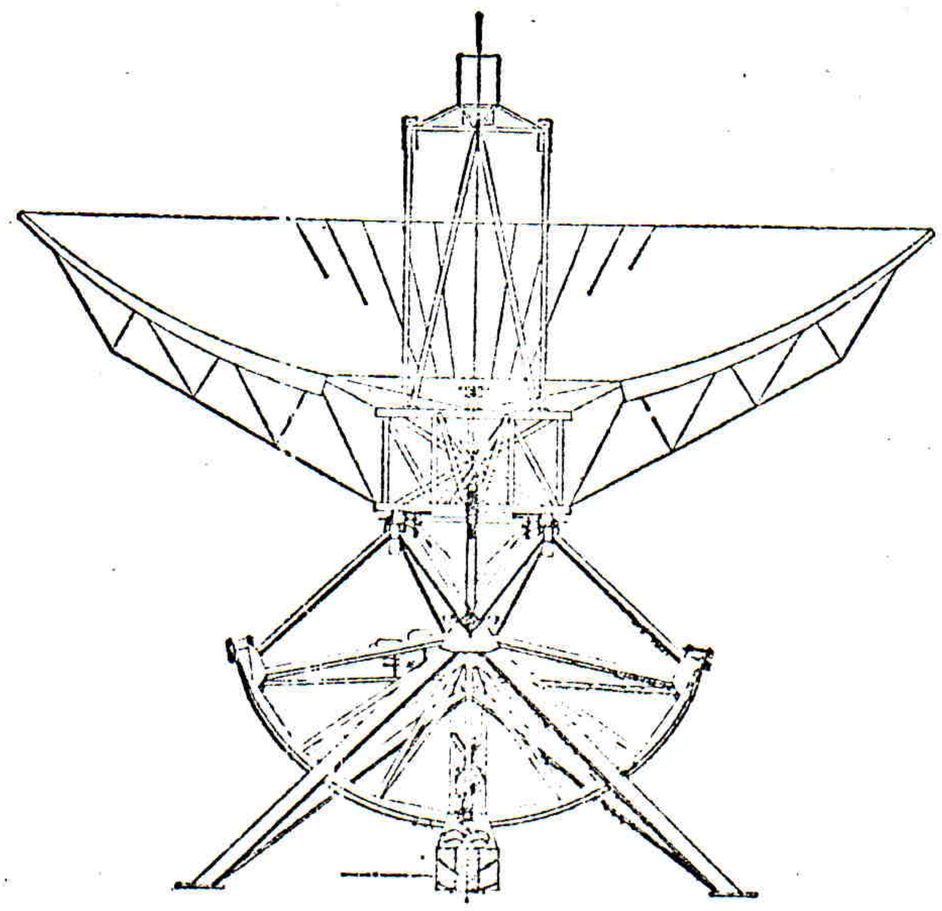

Fig. 3. Drawing of single antenna seen from the north.